Journal of Computational Physics 228 (2009) 4945–4960

Contents lists available at ScienceDirect

Journal of Computational Physics

journal homepage: www.elsevier.com/locate/jcp

The finite volume local evolution Galerkin method for solving the hyperbolic conservation laws

Yutao Sun, Yu-Xin Ren *

Department of Engineering Mechanics, Tsinghua University, Beijing 100084, China

ARTICLE INFO

Article history:
Received 14 May 2008
Received in revised form 31 March 2009
Accepted 4 April 2009
Available online 11 April 2009

MSC:
65M06
76N15
35L65

Keywords:
Multi-dimensional upwind scheme
Finite volume scheme
Euler equations
The finite volume local evolution Galerkin method

ABSTRACT

This paper presents a finite volume local evolution Galerkin (FVLEG) scheme for solving the hyperbolic conservation laws. The FVLEG scheme is the simplification of the finite volume evolution Galerkin method (FVEG). In FVEG, a necessary step is to compute the dependent variables at cell interfaces at $t_n + \tau$ ($0 < \tau \leqslant \Delta t$). The FVLEG scheme is constructed by taking $\tau \to 0$ in the evolution operators of FVEG. The FVLEG scheme greatly simplifies the evaluation of the numerical fluxes. It is also well suited with the semi-discrete finite volume method, making the flux evaluation being decoupled with the reconstruction procedure while maintaining the genuine multi-dimensional nature of the FVEG methods. The derivation of the FVLEG scheme is presented in detail. The performance of the proposed scheme is studied by solving several test cases. It is shown that FVLEG scheme can obtain very satisfactory numerical results in terms of accuracy and resolution.

1. Introduction

The numerical solutions of systems of hyperbolic conservation laws have been dominated by Riemann-solver-based schemes since the work of Godunov [4], Van Leer [22], Harten–Lax [5], Osher and Solomon [15] and Roe [17]. This approach, known as flux-difference splitting (FDS), has the desirable property of accurately resolving shock waves as well as contact discontinuities. When extending the flux-difference schemes to multi-dimensional problems, the so-called grid aligned finite volume approach or dimensional splitting method is adopted traditionally using one-dimensional Riemann solvers. However, for multi-dimensional problem, there is in general no longer a finite number of directions of information propagation. Roe [18] has pointed out that the approach based on one-dimensional Riemann solvers may lead to a misinterpretation of the local wave structure of the solution. In fact, it turned out that in certain cases, e.g. when there are strong shocks or waves are propagating in directions that are oblique with respect to the mesh, this approach leads to structural deficiencies and large errors in the solutions [8,16].

To overcome the drawbacks of existing methods based on dimensional splitting or the "grid-aligned" approaches, there have been considerable efforts to develop so-called "genuinely multi-dimensional schemes" for solving hyperbolic conservation laws in recent years [2,3,6,14]. While we are not in the position to give a detailed review of these schemes, we would

* Corresponding author. Tel.: +86 10 62785543; fax: +86 10 62781824.
E-mail address: ryx@tsinghua.edu.cn (Y.-X. Ren).

0021-9991/$ - see front matter © 2009 Elsevier Inc. All rights reserved.
doi:10.1016/j.jcp.2009.04.001

like to draw the readers' attention to the genuinely multi-dimensional finite volume evolution Galerkin (FVEG) method [11] which is also the starting point of the present paper.

The finite volume evolution Galerkin (FVEG) schemes can be considered as a generalization of the original idea of Godunov to multi-dimensional hyperbolic conservation laws within the framework of the finite volume approach. To construct genuinely multi-dimensional schemes, the exact integral equations from a general theory of bicharacteristics for linear (or linearized) hyperbolic systems were derived. These integral equations were further approximated by approximate evolution operators in such a way that all of the infinitely many directions of propagation of bicharacteristics were explicitly taken into account. These approximate evolution operators were then used to compute the interfacial dependent variables for the evaluation of the numerical fluxes.

The FVEG schemes have been studied extensively from theoretical as well as numerical point of view and applied to various applications [9,10,12,21]. It is shown that the FVEG schemes yield better accuracy and resolution than some well known finite difference and finite volume schemes. However, theses schemes are more complicated in implementation than traditional finite volume schemes. For two-dimensional FVEG schemes, the numerical fluxes across cell interfaces are computed preferably by the Simpson rule. The use of the Simpson rule takes the multi-dimensional effects at cell vertices into account and is beneficial to the monotonicity of the scheme [9]. Using this approach, the complication comes mainly from the evaluation of the values of the dependent variables at $t_n + \tau$ $(0 < \tau \leqslant \Delta t)$ at the midpoint and two corner points of a cell interface. In practice, these interfacial values of the dependent variables are evaluated by certain approximate evolution operators which involve the integrals around the Mach cones. These integrals can be computed exactly as well as numerically. However, for slant Mach cones associated with the nonlinear hyperbolic systems (e.g. the Euler equations), the exact evaluation of the integrals leads to very lengthy and tedious computations, especially when reconstructions with higher order polynomials are adopted in the finite volume schemes. Using numerical integrations may simplify the computation; however, it also leads to an increase of computational cost and/or a decrease of accuracy especially when the reconstruction functions are discontinuous at cell interfaces.

In the present paper, a finite volume local evolution Galerkin (FVLEG) method is proposed. The FVLEG method is a combination of the FVEG method and the semi-discrete finite volume scheme, in which a necessary step is to let $\tau \to 0$ in the evolution operators of FVEG. It is shown that the FVLEG approach greatly simplifies the evaluation of numerical fluxes and also makes it straightforward to apply the FVLEG scheme on general shaped control volumes. Furthermore, because of the semi-discrete nature of the present method, the flux evaluation is decoupled with the reconstruction procedure and time integration is independent of the spatial discretiztion. These properties are important in constructing both temporally and spatially higher order schemes. The performance of the proposed scheme is studied by solving several test cases. It is shown that FVLEG scheme can obtain very good numerical results in terms of both accuracy and resolution.

2. The finite volume schemes

2.1. The governing equations

Although the FVEG schemes can be applied to general hyperbolic conservation laws, we consider here the two-dimensional Euler equations describing the compressible inviscid flows without a loss of the generality. In conservation form the Euler equations are

$$\frac{\partial \mathbf{U}}{\partial t} + \frac{\partial \mathbf{F}}{\partial x} + \frac{\partial \mathbf{G}}{\partial y} = 0, \tag{1}$$

where $\mathbf{U}$ is the vector of the conserved variables given as $\mathbf{U} = [\rho, \rho u, \rho v, \rho E]^{\mathrm{T}}$. The detailed formulations of the flux terms are well known and are omitted here for brevity.

2.2. The finite volume scheme

We consider some two-dimensional domain in x–y space and assume that it is discretized into structured quadrilateral control volumes. Examples of typical control cells are shown in Fig. 1. Finite volume schemes for Eq. (1) are obtained by considering the control volume balance equations

$$\frac{\partial}{\partial t}\int\int_{\Omega_{ij}} \mathbf{U}_{ij}\, dx\, dy + \oint_{\partial\Omega_{ij}} \mathbf{H}\cdot\mathbf{n}\, dl = 0, \tag{2}$$

where Ω_{ij} is the control volume, $\partial\Omega_{ij}$ is the boundary of Ω_{ij}, $\mathbf{H} = \mathbf{F}\mathbf{i} + \mathbf{G}\mathbf{j}$ is the tensor of the fluxes. $\mathbf{n} = n_x\mathbf{i} + n_y\mathbf{j}$ is the outward unit vector normal to the surface $\partial\Omega_{ij}$. On a quadrilateral control volume with its faces denoted by $I_k = I_{i+\alpha(k),j+\beta(k)}$ $(k = 1,\ldots,4)$, where $\alpha(k) = \frac{1}{2}\sin\left(\frac{(k-2)\pi}{2}\right), \beta(k) = \frac{1}{2}\cos\left(\frac{k\pi}{2}\right)$, the finite volume balance equations can be written as

$$\frac{\partial \overline{\mathbf{U}}_{ij}}{\partial t} = -\frac{1}{\overline{\Omega}_{ij}}\sum_{k=1}^{4}\int_{I_k} \mathbf{H}\cdot\mathbf{n}\, dl, \tag{3}$$

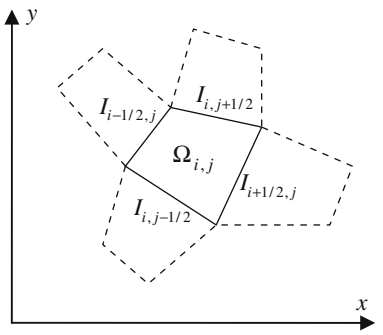

Fig. 1. The control volumes in the finite volume approach.

where

$$\overline{\mathbf{U}}_{ij} = \frac{\iint_{\Omega_{ij}} \mathbf{U}\,dx\,dy}{\overline{\Omega}_{ij}} \quad \text{and} \quad \overline{\Omega}_{ij} = \int\int_{\Omega_{ij}} dx\,dy \tag{4}$$

are, respectively, the cell average of the conservative variables and cell volume. $\int_{l_k} \mathbf{H}\cdot\mathbf{n}\,dl$ is the flux across I_k ($k = 1,\ldots,4$).

There are basically two approaches to handle the time integration. The first one is the fully discrete approach for which Eq. (3) is further integrated in time from t_n to $t_{n+1} = t_n + \Delta t$ to get

$$\overline{\mathbf{U}}_{ij}^{n+1} = \overline{\mathbf{U}}_{ij}^{n} - \frac{1}{\overline{\Omega}_{ij}} \sum_{k=1}^{4} \int_{t_n}^{t_n+\Delta t} \left(\int_{I_k} \mathbf{H}\cdot\mathbf{n}\,dl \right) dt. \tag{5}$$

For a temporally second-order scheme, the time integration can be approximated by the midpoint rule so that

$$\overline{\mathbf{U}}_{ij}^{n+1} = \overline{\mathbf{U}}_{ij}^{n} - \frac{\Delta t}{\overline{\Omega}_{ij}} \sum_{k=1}^{4} \int_{I_k} \mathbf{H}(E_{\Delta t/2} R_\Omega \overline{\mathbf{U}}^n)\cdot\mathbf{n}\,dl. \tag{6}$$

In Eq. (6), R_Ω is the reconstruction operator which transforms the cell averages of the conservative variables to their spatial distributions usually in terms of the piecewise polynomial functions; $E_{\Delta t/2}$ is the approximate evolution operator to compute the intermediate value of the solution at $t_{n+1/2} = t_n + \Delta t/2$ on cell interface I_k using $R_\Omega\overline{\mathbf{U}}^n$ as the initial condition. We note this is the approach adopted in the FVEG schemes.

The second one is the semi-discrete (method of line) approach which is the one adopted in the present paper. In this approach, Eq. (3) is treated as a system of ordinary differential equations (ODEs) with respect to the time after the spatial discretization. And the system of ODEs is integrated with a certain algorithm to obtain the numerical solutions. For example, the second-order Runge–Kutta scheme of Heun can be used for a temporally second-order finite volume scheme:

$$\begin{aligned}
&\overline{\mathbf{U}}_{ij}^{(0)} = \overline{\mathbf{U}}_{ij}^{n},\\
&\overline{\mathbf{U}}_{ij}^{(1)} = \overline{\mathbf{U}}_{ij}^{(0)} - \frac{\Delta t}{\overline{\Omega}_{ij}} \sum_{k=1}^{4} \int_{I_k} \mathbf{H}(E_0 R_\Omega \overline{\mathbf{U}}^{(0)})\cdot\mathbf{n}\,dl,\\
&\overline{\mathbf{U}}_{ij}^{(2)} = \frac{1}{2}\overline{\mathbf{U}}_{ij}^{(0)} + \frac{1}{2}\left(\overline{\mathbf{U}}_{ij}^{(1)} - \frac{\Delta t}{\overline{\Omega}_{ij}} \sum_{k=1}^{4} \int_{I_k} \mathbf{H}(E_0 R_\Omega \overline{\mathbf{U}}^{(1)})\cdot\mathbf{n}\,dl \right),\\
&\overline{\mathbf{U}}_{ij}^{n+1} = \overline{\mathbf{U}}_{ij}^{(2)},
\end{aligned} \tag{7}$$

where E_0 is the approximate evolution operator to compute the solution at $t_n^+ = t_n + 0$ on cell interface I_k. It clear that for the semi-discrete finite volume scheme, the interfacial dependent variables need only to be evolved for an infinite small period of time to compute the numerical fluxes, whereas for the fully discrete approach, the interfacial dependent variables need to be evolved for an finite period of time. We will see in Section 4 that the use of the semi-discrete approach greatly simplifies the evaluation of numerical fluxes and makes it straightforward to apply the numerical scheme on general shaped control volumes.

To complete a finite volume scheme, we must choose or construct the specific forms of the reconstruction operator, the approximate evolution operator ($E_{\Delta t/2}$ or E_0) and the numerical integration operator to approximate the flux $\int_{l_k} \mathbf{H}\cdot\mathbf{n}\,dl$. In the rest part of this section will present the procedures for reconstruction and approximate integration of the numerical fluxes, while the approximate evolution operator E_0 used in the present paper will be discussed in detail in Section 4 after a brief review of the approximate evolution operator $E_{\Delta t/2}$ of FVEG in Section 3.

2.3. The reconstructions

In the framework of the finite volume method, it is necessary to reconstruct a piecewise polynomial function, $\mathbf{U}(x,y,t)$, from the cell average data $\overline{\mathbf{U}}_{i,j}$. The simplest reconstruction is the 0th order reconstruction, which is

$$\mathbf{U}(x,y,t)|_{(x,y)\in\Omega_{i,j}} = \overline{\mathbf{U}}_{ij}. \tag{8}$$

The 0th order reconstruction leads to a spatially first-order scheme. For a second-order scheme, a piecewise linear reconstruction is sufficient. In the present paper, the reconstruction procedure of [19] is used. In this procedure, the reconstruction is carried out in terms of primitive variables $\mathbf{V} = (\rho,u,v,p)^T$. The gradient of primitive variables, $\nabla\mathbf{W}^n_{i,j}$, is evaluated using the Gauss theorem:

$$\nabla\mathbf{V}_{i,j} \approx \frac{1}{\overline{\Omega}_{i,j}} \sum_{k=1}^{4} \mathbf{V}_k \mathbf{n}_k \Delta l_k, \tag{9}$$

where the Δl_k is the length of the cell face I_k. The primitive variables at cell interfaces, $I_{i\pm1/2,j}$ for instance, are computed by

$$\mathbf{V}_{i+1/2j} = \overline{\mathbf{V}}_{i,j} + \frac{1}{2} L\left(\overline{\mathbf{V}}_{i+1,j} - \overline{\mathbf{V}}_{i,j}, \overline{\mathbf{V}}_{i,j} - \overline{\mathbf{V}}_{i-1,j}\right),$$
$$\overline{\mathbf{V}}_{i-1/2j} = \overline{\mathbf{V}}_{i,j} - \frac{1}{2} L\left(\overline{\mathbf{V}}_{i+1,j} - \overline{\mathbf{V}}_{i,j}, \overline{\mathbf{V}}_{i,j} - \overline{\mathbf{V}}_{i-1,j}\right),$$

where L is the slope limiter which is similar to the smoothness indicator of [20]

$$L(a,b) = \frac{\max(ab,0)(a+b)}{a^2+b^2}. \tag{10}$$

Using this gradient, the piecewise linear reconstruction in $\Omega_{i,j}$ is expressed as

$$\mathbf{V}(x,y,t)|_{(x,y)\in\Omega_{i,j}} = \overline{\mathbf{V}}_{ij} + \left(\frac{\partial\mathbf{V}}{\partial x}\right)_{i,j}(x-x_{ij}) + \left(\frac{\partial\mathbf{V}}{\partial y}\right)_{i,j}(y-y_{ij}). \tag{11}$$

It should be noted that this reconstruction procedure is valid only for the structured grids. Other reconstruction procedure is needed if the numerical scheme of the present paper is intended to be applied on the unstructured meshes.

2.4. The approximate cell interface integral

In the FVEG approach, the flux $\int_{I_k}\mathbf{H}(E_{\Delta t/2}R_\Omega\overline{\mathbf{U}}^n)\cdot\mathbf{n}\,dl$ is preferably approximated by the Simpson rule, namely

$$\int_{I_k}\mathbf{H}(E_{\Delta t/2}R_\Omega\overline{\mathbf{U}}^n)\cdot\mathbf{n}\,dl \approx \left(\mathbf{H}\left(E^{k,1}_{\Delta t/2}R_\Omega\overline{\mathbf{U}}^n\right) + 4\mathbf{H}\left(E^{k,c}_{\Delta t/2}R_\Omega\overline{\mathbf{U}}^n\right) + \mathbf{H}\left(E^{k,2}_{\Delta t/2}R_\Omega\overline{\mathbf{U}}^n\right)\right)\cdot\mathbf{n}_k\Delta l_k/6, \tag{12}$$

where Δl_k is the length of the I_k interface, the superscripts $(k,1)$, $(k,2)$ represent two end points of I_k interface and the superscript (k,c) stands for the midpoint of the I_k interface. It is shown in [9,10] that the use of the Simpson rule to approximate the cell interface integral in the flux computation can lead to a scheme which is monotonic under some conditions. Moreover, it takes multi-dimensional effects from the corners into account. In the present paper, we use the same approach to handle the flux integration which can be written as

$$\int_{I_k}\mathbf{H}(E_0R_\Omega\overline{\mathbf{U}})\cdot\mathbf{n}\,dl \approx \left(\mathbf{H}\left(E^{k,1}_0R_\Omega\overline{\mathbf{U}}\right) + 4\mathbf{H}\left(E^{k,c}_0R_\Omega\overline{\mathbf{U}}\right) + \mathbf{H}\left(E^{k,2}_0R_\Omega\overline{\mathbf{U}}\right)\right)\cdot\mathbf{n}_k\Delta l_k/6 \tag{13}$$

in the framework of the semi-discrete finite volume scheme.

3. A brief review of the FVEG schemes

The central idea of FVEG methods is to construct $E_{\Delta t/2}$ for evaluating the numerical fluxes through cell interfaces using the theory of bicharacteristics in a finite volume scheme. In this section, we recall the work of Lukáčová-Medvid'ová et al. [8,9,11,12] to present the basic idea of the FVEG schemes and to introduce the notations that will be used in deriving the FVLEG scheme. For this purpose, it is convenient to start with the Euler equations in primitive variable form,

$$\mathbf{V}_t + \mathbf{A}_1(\mathbf{V})\mathbf{V}_x + \mathbf{A}_2(\mathbf{V})\mathbf{V}_y = 0, \tag{14}$$

where

$$\mathbf{V} = \begin{pmatrix}\rho\\ u\\ v\\ p\end{pmatrix}, \quad \mathbf{A}_1 = \begin{pmatrix}u & \rho & 0 & 0\\ 0 & u & 0 & \frac{1}{\rho}\\ 0 & 0 & u & 0\\ 0 & \gamma p & 0 & u\end{pmatrix}, \quad \mathbf{A}_2 = \begin{pmatrix}v & 0 & \rho & 0\\ 0 & v & 0 & 0\\ 0 & 0 & v & \frac{1}{\rho}\\ 0 & 0 & \gamma p & v\end{pmatrix}.$$

To simplify the construction of $E_{\Delta t/2}$, the system of Euler equations is linearized by freezing the Jacobian matrices about a reference state $\tilde{\mathbf{V}} = (\tilde{\rho}, \tilde{u}, \tilde{v}, \tilde{p})$ at point $\tilde{\mathbf{P}} = (\tilde{x}, \tilde{y}, \tilde{t})$. The linearized system with frozen constant Jacobian matrices can be written as

$$\mathbf{V}_t + \mathbf{A}_1(\tilde{\mathbf{V}})\mathbf{V}_x + \mathbf{A}_2(\tilde{\mathbf{V}})\mathbf{V}_y = 0. \tag{15}$$

Using the characteristic theory, Eq. (15) can be transformed in to the following quasi-diagonalized system:

$$\mathbf{W}_t + \mathbf{\Lambda}_1\mathbf{W}_x + \mathbf{\Lambda}_2\mathbf{W}_y = \mathbf{S}, \tag{16}$$

where

$$\mathbf{W} = \begin{pmatrix} w_1 \\ w_2 \\ w_3 \\ w_4 \end{pmatrix} = \begin{pmatrix} \frac{1}{2}\left(-\frac{p}{\rho a} + u\cos\theta + v\sin\theta\right) \\ \rho - \frac{p}{a^2} \\ u\sin\theta - v\cos\theta \\ \frac{1}{2}\left(\frac{p}{\rho a} + u\cos\theta + v\sin\theta\right) \end{pmatrix},$$

$$\mathbf{\Lambda}_1 = diag(\lambda_{1,1}(\theta), \ldots, \lambda_{1,4}(\theta)) = \begin{pmatrix} \tilde{u} - \tilde{a}\cos\theta & 0 & 0 & 0 \\ 0 & \tilde{u} & 0 & 0 \\ 0 & 0 & \tilde{u} & 0 \\ 0 & 0 & 0 & \tilde{u} + \tilde{a}\cos\theta \end{pmatrix},$$

$$\mathbf{\Lambda}_2 = diag(\lambda_{2,1}(\theta), \ldots, \lambda_{2,4}(\theta)) = \begin{pmatrix} \tilde{v} - \tilde{a}\cos\theta & 0 & 0 & 0 \\ 0 & \tilde{v} & 0 & 0 \\ 0 & 0 & \tilde{v} & 0 \\ 0 & 0 & 0 & \tilde{v} + \tilde{a}\cos\theta \end{pmatrix},$$

$$\mathbf{S} = \begin{pmatrix} s_1 \\ s_2 \\ s_3 \\ s_4 \end{pmatrix} = \begin{pmatrix} \frac{1}{2}\tilde{a}\left(\sin\theta\frac{\partial w_3}{\partial x} - \cos\theta\frac{\partial w_3}{\partial y}\right) \\ 0 \\ \tilde{a}\sin\theta\left(\frac{\partial w_1}{\partial x} - \frac{\partial w_4}{\partial x}\right) - \tilde{a}\cos\theta\left(\frac{\partial w_1}{\partial y} - \frac{\partial w_4}{\partial y}\right) \\ \frac{1}{2}\tilde{a}\left(-\sin\theta\frac{\partial w_3}{\partial x} + \cos\theta\frac{\partial w_3}{\partial y}\right) \end{pmatrix}$$

and $\tilde{a} = \sqrt{\gamma\tilde{p}/\tilde{\rho}}$ is the speed of sound.

Eq. (16) shows that each characteristic variable w_l is evolved along the corresponding bicharacteristic curve

$$\left(\frac{d\mathbf{r}}{dt}\right)_l = (\lambda_{1,l}(\theta), \lambda_{2,l}(\theta))^T, \tag{17}$$

where $\mathbf{r} = (x,y)^T$, according to the relation

$$\frac{Dw_l}{Dt} = \frac{\partial w_l}{\partial t} + \lambda_{1,l}(\theta)\frac{\partial w_l}{\partial x} + \lambda_{1,l}(\theta)\frac{\partial w_l}{\partial y} = s_l. \tag{18}$$

Therefore, given the initial condition at time t, the solution of w_l at $\mathbf{P} = (x,y,t+\tau)$ is

$$w_l(x,y,t+\tau,\theta) = w_l(x - \lambda_{1,l}(\theta)\tau, y - \lambda_{2,l}(\theta)\tau, t) + s'_l(\theta), \tag{19}$$

where

$$s'_l(\theta) = \int_t^{t+\tau} s_l(x - \lambda_{1,l}(\theta)(t+\tau-\varsigma), y - \lambda_{2,l}(\theta)(t+\tau-\varsigma), \varsigma)d\varsigma. \tag{20}$$

For any given angle θ, the four bicharacteristic curves from P denoted by $C_l(\theta)$, $l = 1,\ldots,4$ are depicted in Fig. 2. The $C_1(\theta)$ or $C_4(\theta)$, for θ from 0 to 2π, generates the so-called Mach cone or the bicharacteristic cone. We denote $Q_l(\theta)$ as the position where $C_l(\theta)$ hits the x–y plane at time t, which, for $l = 1,\ldots,4$, is given by

$$\begin{aligned} Q_1(\theta) &= (x - (\tilde{u} - \tilde{a}\cos\theta)\tau, y - (\tilde{v} - \tilde{a}\sin\theta)\tau, t), \\ Q_2(\theta) &= Q_3(\theta) = (x - \tilde{u}\tau, y - \tilde{v}\tau, t), \\ Q_4(\theta) &= (x - (\tilde{u} + \tilde{a}\cos\theta)\tau, y - (\tilde{v} + \tilde{a}\sin\theta)\tau, t). \end{aligned} \tag{21}$$

Using these notations, Eq. (19) can be also written as

$$w_l(P,\theta) = w_l(Q_l(\theta)) + s'_l(\theta) \tag{22}$$

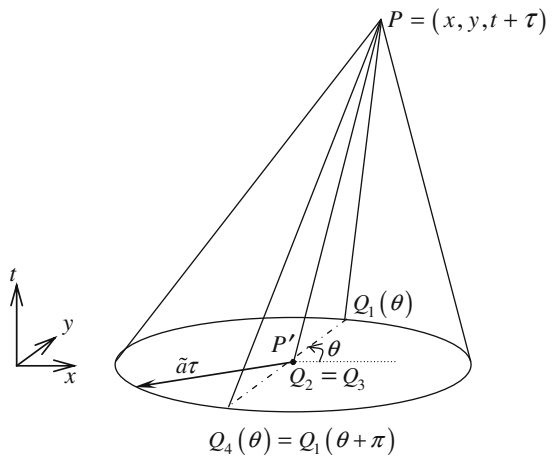

Fig. 2. The bicharacteristic curves and the Mach cone.

or in vector form as

$$\mathbf{W}(P,\theta)=\begin{pmatrix} w_1(Q_1(\theta)) \\ w_2(Q_2(\theta)) \\ w_3(Q_3(\theta)) \\ w_4(Q_4(\theta)) \end{pmatrix}+\begin{pmatrix} s_1'(\theta) \\ s_2'(\theta) \\ s_3'(\theta) \\ s_4'(\theta) \end{pmatrix}. \tag{23}$$

For $\theta\in(0,2\pi)$, both $Q_1(\theta)$ and $Q_4(\theta)$ are circles with radius of $\tilde{a}\tau$ and center at $(x-\tilde{u}\tau, y-\tilde{v}\tau, t)$. It is also obvious that $Q_4(\theta)=Q_1(\theta+\pi)$. $Q_2(\theta)=Q_3(\theta)$ are point at the center of $Q_1(\theta)$ and $Q_4(\theta)$. Multiplication of Eq. (23) with **R** from the left and integration with respect θ from 0 to 2π leads to:

$$\mathbf{V}(P)=\frac{1}{2\pi}\int_0^{2\pi}\left(\sum_{l=1}^{4}\mathbf{r}_l[w_l(Q_l(\theta))+s_l'(\theta)]\right)d\theta. \tag{24}$$

In [11], the symmetries in the characteristic variables and the source terms were used to get the detailed expressions of the solution in terms of the primitive variables

$$\begin{aligned}\rho(P)=\rho(P')-\frac{p(P')}{\tilde{a}^2}+\frac{1}{2\pi}\int_0^{2\pi}\left[\frac{p(Q)}{\tilde{a}^2}-\frac{\tilde{\rho}}{\tilde{a}}u(Q)\cos\theta-\frac{\tilde{\rho}}{\tilde{a}}v(Q)\sin\theta\right]d\theta-\frac{\tilde{\rho}}{\tilde{a}}\frac{1}{2\pi}\int_0^{2\pi}\int_t^{t+\tau}S(\mathbf{r}-[\tilde{\mathbf{u}}-\tilde{a}\mathbf{n}(\theta)]\\ \times(t+\tau-\zeta),\zeta,\theta)d\zeta\,d\theta,\end{aligned} \tag{25}$$

$$\begin{aligned}u(P)=\frac{1}{2\pi}\int_0^{2\pi}\left[-\frac{p(Q)}{\tilde{\rho}\tilde{a}}\cos\theta+u(Q)\cos^2\theta+v(Q)\sin\theta\cos\theta\right]d\theta+\frac{1}{2\pi}\int_0^{2\pi}\int_t^{t+\tau}\cos\theta S(\mathbf{r}-[\tilde{\mathbf{u}}-\tilde{a}\mathbf{n}(\theta)]\\ \times(t+\tau-\zeta),\zeta,\theta)d\zeta\,d\theta+\frac{1}{2}u(P')-\frac{1}{2\tilde{\rho}}\int_t^{t+\tau}p_x(\mathbf{r}-\tilde{\mathbf{u}}\times(t+\tau-\zeta),\zeta)d\zeta,\end{aligned} \tag{26}$$

$$\begin{aligned}v(P)=\frac{1}{2\pi}\int_0^{2\pi}\left[-\frac{p(Q)}{\tilde{\rho}\tilde{a}}\sin\theta+u(Q)\cos\theta\sin\theta+v(Q)\sin^2\theta\right]d\theta+\frac{1}{2\pi}\int_0^{2\pi}\int_t^{t+\tau}\sin\theta S(\mathbf{r}-[\tilde{\mathbf{u}}-\tilde{a}\mathbf{n}(\theta)]\\ \times(t+\tau-\zeta),\zeta,\theta)d\zeta\,d\theta+\frac{1}{2}v(P')-\frac{1}{2\tilde{\rho}}\int_t^{t+\tau}p_y(\mathbf{r}-\tilde{\mathbf{u}}\times(t+\tau-\zeta),\zeta)d\zeta,\end{aligned} \tag{27}$$

$$p(P)=\frac{1}{2\pi}\int_0^{2\pi}[p(Q)-\tilde{\rho}\tilde{a}u(Q)\cos\theta-\tilde{\rho}\tilde{a}v(Q)\sin\theta]d\theta-\tilde{\rho}\tilde{a}\frac{1}{2\pi}\int_0^{2\pi}\int_t^{t+\tau}S(\mathbf{r}-[\tilde{\mathbf{u}}-\tilde{a}\mathbf{n}(\theta)]\times(t+\tau-\zeta),\zeta,\theta)d\zeta\,d\theta, \tag{28}$$

where the source term S is given by

$$S(\mathbf{r},t,\theta):=\tilde{a}[u_x(\mathbf{r},t,\theta)\sin^2\theta-(u_y(\mathbf{r},t,\theta)+v_x(\mathbf{r},t,\theta))\times\sin\theta\cos\theta+v_y(\mathbf{r},t,\theta)\cos^2\theta], \tag{29}$$

and

$$\mathbf{r}-[\tilde{\mathbf{u}}-\tilde{a}\mathbf{n}(\theta)]\times(t+\tau-\zeta)=(x-(\tilde{u}-\tilde{a}\cos\theta)(t+\tau-\zeta),y-(\tilde{u}-\tilde{a}\cos\theta)(t+\tau-\zeta)).$$

We note that the notations $Q = Q_1(\theta)$ and $P' = Q_2$ adopted in Ref. [11] are used in Eqs. (25)–(28). Eqs. (25)–(28) are exact integral equations for the solution to the linearized Euler equations (8). It is currently impossible to get an explicit solution of these equations. Therefore, certain approximate operators which are termed as EG1 through EG5 in [11,12,23] have been constructed to get the approximate explicit solutions. These approximate solutions are the basis of the FVEG method. When these approximate evolution operators with $\tau = \Delta t/2$ are applied to the piecewise polynomial data obtained by the reconstruction procedure, these approximate solutions are served as $E_{\Delta t/2} R_\Omega \bar{\mathbf{U}}^n$ in Eq. (6). We will not review the detailed derivation of EG1 through EG5 in the present paper for brevity. However, some of the approximations will be used or extended in Section 4 of the present paper when designing the FVLEG method.

4. The finite volume local evolution Galerkin method

In the present paper, the finite volume local evolution Galerkin (FVLEG) method will be presented. The idea behind FVLEG is very simple. If we set $\tau = 0$ in Eq. (24) (or Eqs. (25)–(28)), it gives the solutions that are evolved for an infinite small period of time from the initial conditions at time t in terms of the primitive variables. In this sense, the FVLEG method is functionally identical to computing the numerical fluxes by using the Riemann solvers in the traditional semi-discrete finite volume methods.

The simplest way to construct the approximate evolution operator E_0 in FVLEG is to set $\tau = 0$ in E_τ, the approximate evolution operator of the FVEG method. In other words, we can use the approximate evolution operators EG1 through EG5 developed in [11,12,23] directly to construct the E_0 by simply taking $\tau = 0$. However, when closely examining the approach for deriving EG1 through EG5, we find that these derivations are highly relied on the Lemma 2.1 of [7]. Strictly speaking, this lemma can be only applied to smooth functions, which is not the case of the present paper. Therefore, in this section, we firstly derive E_τ using a new lemma which is similar to Lemma 2.1 but applicable to piecewise smooth functions, and then we construct E_0 according to E_τ.

4.1. E_τ

In this section, we will describe the derivation of the approximate evolution operator E_τ at a vertex of the control volumes. For the structured quadrilateral grids, there are four control volumes around the vertex $\mathbf{r} = (x,y)^T$ which is shown in Fig. 3(a). For a more general case such as the unstructured grids shown in Fig. 3(b), we assume there are M control volumes with a common vertex $\mathbf{r} = (x,y)^T$. In this case, we need to construct E_τ at $\mathbf{r} = (x,y)^T$ which is the endpoint of M rays that are separated by M control volumes. In this sense, the approximate evolution operator at the center of a cell interface can be viewed as a special case of that at a cell vertex, which is the endpoint of two rays separated by two control volumes shown in Fig. 3(c). We consider the general case, in which we assume the circle Q at time t corresponding to the Mach cone with its apex at $P = (x,y,t+\tau)$ is divided by the M rays with the common vertex $\mathbf{r} = (x,y)^T$ into N segments of arc, which is shown in Fig. 4 for the structured quadrilateral grid case. For the ith arc, its starting and ending angles are denoted by θ_{ib} and θ_{ie}, respectively. The θ_{ib} and θ_{ie} can be obtained from the geometry of the control volume and Eq. (21). It should be noted that the determination of θ_{ib} and θ_{ie} is far from trivial since there are many possible ways of intersections depending on the reference state $\tilde{\mathbf{V}} = (\tilde{\rho}, \tilde{u}, \tilde{v}, \tilde{p})$ at $\mathbf{r} = (x,y)^T$and geometries of the control volumes. Nevertheless, this is a purely geometrical problem and can be solved without any principle difficulties. The procedure to determine θ_{ia} and θ_{ib} is presented in Appendix of the present paper. After the determination of θ_{ia} and θ_{ib}, Eqs. (25)–(28) can be rewritten into

$$\begin{aligned}\rho(P) = \rho(P') &- \frac{p(P')}{\tilde{a}^2} + \frac{1}{2\pi}\sum_{i=1}^{N}\int_{\theta_{ib}}^{\theta_{ie}}\left[\frac{P(Q)}{\tilde{a}^2} - \frac{\tilde{\rho}}{\tilde{a}}u(Q)\cos\theta - \frac{\tilde{\rho}}{\tilde{a}}v(Q)\sin\theta\right]d\theta \\ &- \frac{\tilde{\rho}}{\tilde{a}}\frac{1}{2\pi}\sum_{i=1}^{N}\int_{\theta_{ib}}^{\theta_{ie}}\left[\int_t^{t+\tau} S(\mathbf{r} - [\tilde{\mathbf{u}} - \tilde{a}\mathbf{n}(\theta)]\times(t+\tau-\zeta),\zeta,\theta)d\zeta\right]d\theta, \end{aligned} \tag{30}$$

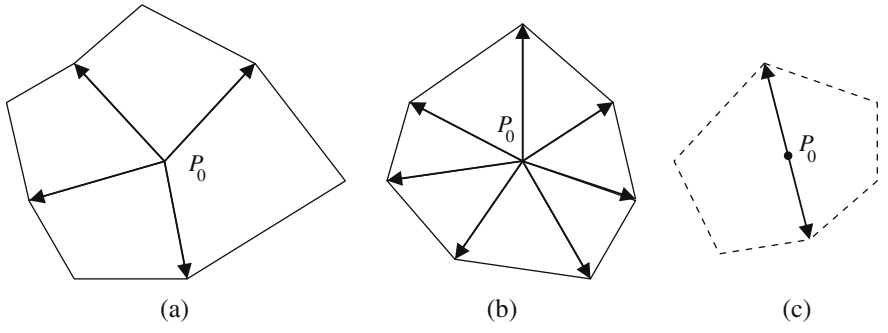

Fig. 3. The locations where the approximate evolution operators E_τ are constructed. (a) The vertex of the control volumes for the structured quadrilateral grid; (b) the vertex of the control volumes for the unstructured grid; (c) the midpoint of the edge of two adjacent control volumes.

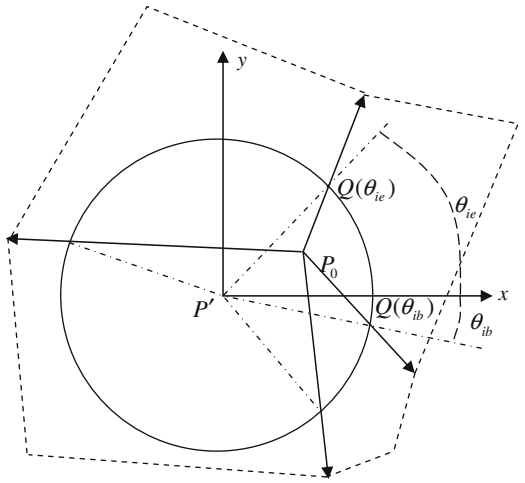

Fig. 4. Possible intersections between the Mach cone and the edges of the control volumes.

$$u(P) = \frac{1}{2\pi}\sum_{i=1}^{N}\int_{\theta_{ib}}^{\theta_{ie}}\left[-\frac{p(Q)}{\tilde{\rho}\tilde{a}}\cos\theta + u(Q)\cos^2\theta + v(Q)\sin\theta\cos\theta\right]d\theta + \frac{1}{2\pi}\sum_{i=1}^{N}\int_{\theta_{ib}}^{\theta_{ie}}\left[\int_{t}^{t+\tau}\cos\theta S(\mathbf{r} - [\tilde{u} - \tilde{a}\mathbf{n}(\theta)]\times(t+\tau-\zeta),\zeta,\theta)d\zeta\right]d\theta + \frac{1}{2}u(P') - \frac{1}{2\tilde{\rho}}\int_{t}^{t+\tau}p_x(\mathbf{r} - \tilde{\mathbf{u}}\times(t+\tau-\zeta),\zeta)d\zeta, \tag{31}$$

$$v(P) = \frac{1}{2\pi}\sum_{i=1}^{N}\int_{\theta_{ib}}^{\theta_{ie}}\left[-\frac{p(Q)}{\tilde{\rho}\tilde{a}}\sin\theta + u(Q)\cos\theta\sin\theta + v(Q)\sin^2\theta\right]d\theta \times \frac{1}{2\pi}\sum_{i=1}^{N}\int_{\theta_{ib}}^{\theta_{ie}}\left[\int_{t}^{t+\tau}\sin\theta S(\mathbf{r} - [\tilde{u} - \tilde{a}\mathbf{n}(\theta)]\times(t+\tau-\zeta),\zeta,\theta)d\zeta\right]d\theta + \frac{1}{2}v(P') - \frac{1}{2\tilde{\rho}}\int_{t}^{t+\tau}p_y(r - \tilde{u}\times(t+\tau-\zeta),\zeta)d\zeta, \tag{32}$$

$$p(P) = \frac{1}{2\pi}\sum_{i=1}^{N}\int_{\theta_{ib}}^{\theta_{ie}}[p(Q) - \tilde{\rho}\tilde{a}u(Q)\cos\theta - \tilde{\rho}\tilde{a}v(Q)\sin\theta]d\theta - \tilde{\rho}\tilde{a}\frac{1}{2\pi}\sum_{i=1}^{N}\int_{\theta_{ib}}^{\theta_{ie}}\left[\int_{t}^{t+\tau}S(\mathbf{r} - [\tilde{u} - \tilde{a}\mathbf{n}(\theta)]\times(t+\tau-\zeta),\zeta,\theta)d\zeta\right]d\theta. \tag{33}$$

To avoid the computation of the integrals $\int_t^{t+\tau}p_x(\mathbf{r} - \tilde{\mathbf{u}}\times(t+\tau-\zeta),\zeta)d\zeta$ and $\int_t^{t+\tau}p_y(\mathbf{r} - \tilde{\mathbf{u}}\times(t+\tau-\zeta),\zeta)d\zeta$ in Eqs. (31) and (32), we use the following relations [11]:

$$\int_{t}^{t+\tau}p_x(\mathbf{r} - \tilde{\mathbf{u}}\times(t+\tau-\zeta),\zeta)d\zeta = -\tilde{\rho}[u(P) - u(P')], \tag{34}$$

$$\int_{t}^{t+\tau}p_y(\mathbf{r} - \tilde{\mathbf{u}}\times(t+\tau-\zeta),\zeta)d\zeta = -\tilde{\rho}[v(P) - v(P')]. \tag{35}$$

Another difficulty in computing Eqs. (30)–(33) arises from the evaluation of the integrals containing the source terms. Here we use the rectangle rule to approximate the time integrals of the source term,

$$\int_{\theta_{ib}}^{\theta_{ie}}\left[\int_{t}^{t+\tau}S(\mathbf{r} - [\tilde{\mathbf{u}} - \tilde{a}\mathbf{n}(\theta)]\times(t+\tau-\zeta),\varsigma,\theta)d\zeta\right]d\theta \approx \tau\int_{\theta_{ib}}^{\theta_{ie}}S(Q(\theta))d\theta, \tag{36}$$

$$\int_{\theta_{ib}}^{\theta_{ie}}\left[\int_{t}^{t+\tau}\cos\theta S(\mathbf{r} - [\tilde{\mathbf{u}} - \tilde{a}\mathbf{n}(\theta)]\times(t+\tau-\zeta),\varsigma,\theta)d\zeta\right]d\theta \approx \tau\int_{\theta_{ib}}^{\theta_{ie}}S(Q(\theta))\cos\theta\,d\theta, \tag{37}$$

$$\int_{\theta_{ib}}^{\theta_{ie}}\left[\int_{t}^{t+\tau}\sin\theta S(\mathbf{r} - [\tilde{\mathbf{u}} - \tilde{a}\mathbf{n}(\theta)]\times(t+\tau-\zeta),\varsigma,\theta)d\zeta\right]d\theta \approx \tau\int_{\theta_{ib}}^{\theta_{ie}}S(Q(\theta))\sin\theta\,d\theta. \tag{38}$$

This approximations have been used in [11] to construct the EG1, EG3 operators. To further simplify the evaluation of Eqs. (36)–(38), the following lemma is introduced [1].

Lemma 4.1. *Suppose* $\omega \in C^1(\mathbb{R}^2)$, and $\phi \in C^1(\mathbb{R})$ *is continuous and differentiable along the arc: A(Q): {Q = (rcos θ, rsin θ); θ ∈ (θ_ib, θ_ie)}. If the integrations are along the arc, we have the following relation:*

$$\phi(\theta_{ie})\omega(Q(\theta_{ie})) - \phi(\theta_{ib})\omega(Q(\theta_{ib})) = \int_{\theta_{ib}}^{\theta_{ie}} \phi'\omega(Q)d\theta - r\int_{\theta_{ib}}^{\theta_{ie}} \phi\left(\sin\theta\frac{\partial\omega}{\partial x} - \cos\theta\frac{\partial\omega}{\partial y}\right)d\theta.$$

This lemma is similar to the Lemma 2.1 of [7]. However, Lemma 2.1 is only applicable to 2π periodic smooth functions. The present lemma is valid for the integrations along an arc. It is then applicable to the integration along a circle with piecewise smooth data. Using this lemma, the evaluation of the integrals containing the source terms in Eqs. (36)–(38) can be greatly simplified. For example, taking $\phi = \sin\theta$, $\omega = u$ and $r = \tilde{a}\tau$, we have

$$\sin(\theta_{ie})u(Q(\theta_{ie})) - \sin(\theta_{ib})u(Q(\theta_{ib})) = \int_{\theta_{ib}}^{\theta_{ie}} \cos\theta u(Q)d\theta - \tilde{a}\tau\int_{\theta_{ib}}^{\theta_{ie}} \sin\theta\left(\sin\theta\frac{\partial u}{\partial x} - \cos\theta\frac{\partial u}{\partial y}\right)d\theta.$$

Similarly, taking $\phi = -\cos\theta$, $\omega = v$, $r = a\tau$, we obtain

$$-\cos(\theta_{ie})v(Q(\theta_{ie})) + \cos(\theta_{ib})v(Q(\theta_{ib})) = \int_{\theta_{ib}}^{\theta_{ie}} \sin\theta v(Q)d\theta + \tilde{a}\tau\int_{\theta_{ib}}^{\theta_{ie}} \cos\theta\left(\sin\theta\frac{\partial v}{\partial x} - \cos\theta\frac{\partial v}{\partial y}\right)d\theta.$$

Therefore,

$$\tau\int_{\theta_{ib}}^{\theta_{ie}} S(Q(\theta))d\theta = \int_{\theta_{ib}}^{\theta_{ie}} (u(Q(\theta))\cos\theta + v(Q(\theta))\sin\theta)d\theta - \sin(\theta_{ie})u(Q(\theta_{ie})) + \cos(\theta_{ie})v(Q(\theta_{ie})) + \sin(\theta_{ib})u(Q(\theta_{ib})) - \cos(\theta_{ib})v(Q(\theta_{ib})). \tag{39}$$

Similarly, we can get

$$\tau\int_{\theta_{ib}}^{\theta_{ie}} S(Q)\sin\theta\,d\theta = \int_{\theta_{ib}}^{\theta_{ie}} (2u(Q(\theta))\sin\theta\cos\theta + v(Q(\theta))(2\sin^2\theta - 1))d\theta - \sin^2\theta_{ie}u(Q(\theta_{ie})) + \sin\theta_{ie}\cos\theta_{ie}v(Q(\theta_{ie})) + \sin^2\theta_{ib}u(Q(\theta_{ib})) - \sin\theta_{ib}\cos\theta_{ib}v(Q(\theta_{ib})) \tag{40}$$

and

$$\tau\int_{\theta_{ib}}^{\theta_{ie}} S(Q)\cos\theta\,d\theta = \int_{\theta_{ib}}^{\theta_{ie}} (u(Q(\theta))(2\cos^2\theta - 1) + 2v(Q(\theta))\sin\theta\cos\theta)d\theta - \sin\theta_{ie}\cos\theta_{ie}u(Q(\theta_{ie})) + \cos^2\theta_{ie}v(Q(\theta_{ie})) + \sin\theta_{ib}\cos\theta_{ib}u(Q(\theta_{ib})) - \cos^2\theta_{ib}v(Q(\theta_{ib})). \tag{41}$$

So far, we have constructed the approximate evolution operator E_τ. When we set $\tau = \Delta t/2$, this operator can be used to compute the numerical fluxes in FVEG schemes. We note the present derivation of the approximate evolution operator E_τ is different with those of [11] in the fact that present method can be applied directly to piecewise smooth data obtained from the reconstruction procedure.

4.2. E_0

To construct E_0, we let $\tau \to 0$ in Eqs. (30)–(33). We note that θ_{ib} and θ_{ie} do not depend on τ. The effects of $\tau \to 0$ is to make $P \to P_0$, $Q \to P_0$ and $P' \to P_0$ where $P_0 = (x,y,t)$; and the length of the arc with two end points $Q(\theta_{ib})$ and $Q(\theta_{ie})$ will tends to zero when $\tau \to 0$. This fact is significant in simplifying the integrals in Eqs. (30)–(33) and (39)–(41), because in this case, we have

$$\mathbf{V}(Q(\theta)) \to \mathbf{V}_i \quad \text{for } \theta_{ib} \leqslant \theta \leqslant \theta_{ie},$$

where $\mathbf{V}_i$ is the vector of the primitive variables at P_0 evaluated in terms of the reconstruction in the control volume containing the arc with two end points $Q(\theta_{ib})$ and $Q(\theta_{ie})$. Therefore, the primitive variables which are the functions of $Q(\theta)$ in Eqs. (30)–(33) and (39)–(41) can be considered as constants for $\theta_{ib} \leqslant \theta \leqslant \theta_{ie}$ and can thus be taken out from the integrals. For example, Eq. (39) can be simplified as

$$\tau\int_{\theta_{ib}}^{\theta_{ie}} S(Q(\theta))d\theta = u_i\int_{\theta_{ib}}^{\theta_{ie}} \cos\theta d\theta + v_i\int_{\theta_{ib}}^{\theta_{ie}} \sin\theta\,d\theta - \sin(\theta_{ie})u_i + \cos(\theta_{ie})v_i + \sin(\theta_{ib})u_i - \cos(\theta_{ib})v_i = 0.$$

It is also easy to prove that

$$\tau\int_{\theta_{ib}}^{\theta_{ie}} S(Q)\sin\theta\,d\theta = 0$$

and

$$\tau \int_{\theta_{ib}}^{\theta_{ie}} S(Q)\cos\theta\, d\theta = 0.$$

The extensive use of this argument in Eqs. (30)–(33) leads to the following formulations:

$$\rho(P) = \rho(P') - \frac{p(P')}{\tilde{a}^2} + \frac{1}{2\pi}\sum_{i=1}^{N}\left[\frac{p_i}{\tilde{a}^2}(\theta_{ie}-\theta_{ib}) - \frac{\tilde{\rho}}{\tilde{a}}u_i(\sin\theta_{ie}-\sin\theta_{ib}) + \frac{\tilde{\rho}}{\tilde{a}}v_i(\cos\theta_{ie}-\cos\theta_{ib})\right], \tag{42}$$

$$u(P) = \frac{1}{\pi}\sum_{i=1}^{N}\left[-\frac{p_i}{\tilde{\rho}\tilde{a}}(\sin\theta_{ie}-\sin\theta_{ib}) + u_i\left(\frac{\theta_{ie}-\theta_{ib}}{2}+\frac{\sin 2\theta_{ie}-\sin 2\theta_{ib}}{4}\right) - v_i\frac{\cos 2\theta_{ie}-\cos 2\theta_{ib}}{4}\right], \tag{43}$$

$$v(P) = \frac{1}{\pi}\sum_{i=1}^{N}\left[\frac{p_i}{\tilde{\rho}\tilde{a}}(\cos\theta_{ie}-\cos\theta_{ib}) - u_i\frac{\cos 2\theta_{ie}-\cos 2\theta_{ib}}{4} + v_i\left(\frac{\theta_{ie}-\theta_{ib}}{2}-\frac{\sin 2\theta_{ie}-\sin 2\theta_{ib}}{4}\right)\right], \tag{44}$$

$$p(P) = \frac{1}{2\pi}\sum_{i=1}^{N}[p_i(\theta_{ie}-\theta_{ib}) - \tilde{\rho}\tilde{a}u_i(\sin\theta_{ie}-\sin\theta_{ib}) + \tilde{\rho}\tilde{a}v_i(\cos\theta_{ie}-\cos\theta_{ib})], \tag{45}$$

which are the specific forms of E_0 for the present paper.

After the construction of E_0, the implementation of the FVLEG method can be summarized as follows.

(1) Reconstruction. The reconstruction procedures of Section 2.3 are used.
(2) Evaluation of the numerical fluxes. In the present paper, the numerical fluxes are computed using Eq. (13) in which the interfacial values of the dependent variables are obtained by applying E_0 on the reconstructed piece-wise polynomial dependent variables.
(3) The time integration. We use the second-order Runge–Kutta scheme, Eq. (7), to solve the system of ODEs resulted from the semi-discrete finite volume approach.

4.3. Remarks

Remark 1. Lemma 4.1 is a key element in constructing E_0. The direct consequence of Lemma 4.1 is that all terms containing $S(\mathbf{r}-[\tilde{\mathbf{u}}-\tilde{a}\mathbf{n}(\theta)]\times(t+\tau-\zeta),\zeta,\theta)$ in Eqs. (30)–(33) vanish in E_0. If Lemma 2.1 of [7] is used instead, these terms are not zero when $\tau\to 0$. We note that the source terms $\mathbf{S}$ in Eq. (16) are not simply set to zero in deriving E_0. In fact, the terms containing p_x and p_y in Eqs. (31) and (32) are parts of $\mathbf{S}$. During the review process of the present paper, we found that the same lemma had been used in [1] for different purpose.

Remark 2. It is interesting to note that in [9,13], the $E_\tau$was designed as the combination of an approximate evolution operator for piecewise constant data (E_τ^{const}) and another approximate evolution operator for continuous bilinear data (E_τ^{bilin}). Although E_τ^{const} is also applied to piecewise smooth data, it is different with the E_τ of the present paper. This can be seen clearly from the construction of E_τ^{const}. In deriving E_τ^{const}, the spatial derivatives such as ϕ_x are approximated by

$$\phi_x(P'(\tilde{t})) \approx \frac{1}{\pi c\tau}\int_0^{2\pi}\varphi(Q(\theta,\tilde{t}))\cos\theta\, d\theta$$

(please refer to [9] for notations); then the integration in above equation is further approximated in order that the E_τ^{const} can produce the exact solution of the one dimensional linear wave equation with piecewise constant data.

Remark 3. Using the procedures of this section, we cast the computation of the integrals in E_τ into the evaluation of θ_{ib} and θ_{ie} in E_0. This practice simplifies the evaluation of the numerical fluxes. Furthermore, the present numerical flux evaluation algorithm is designed to be applied on general shaped control volumes. Eqs. (42)–(45) are very general and can be applied on both structured and unstructured meshes.

Remark 4. The present scheme is a semi-discrete finite volume scheme in which the spatial accuracy is solely determined by the reconstruction procedures. If a higher order reconstruction is used, the present scheme can achieve higher spatial accuracy. For the FVLEG scheme, the E_0 is independent of the reconstruction procedures. On the other hand, the E_τ in the FVEG schemes is closely related to the reconstruction procedures, which makes it more complicate to extend the FVEG schemes to higher order of accuracy.

5. Numerical tests

In this section, several test cases are presented to verify the accuracy as well as the shock capturing capability of the present scheme. It is reported that the FVEG schemes using some of the approximate evolution operators (EG1–EG4) did not provide full stability for a CFL number of 1 [9]. However, the numerical tests show that the present scheme is stable up to a CFL number of 1 when the second-order Runge–Kutta method is used for time integration. In all the test cases of this section, the CFL number is taken as 0.8.

5.1. Accuracy

We use two test cases to study the accuracy of the present numerical scheme. The first test case is taken from [6]. The initial condition has zero velocity and radially symmetric ρ and E which are expressed as

$$\rho(x,y,0) = E(x,y,0) = \begin{cases} 1 - 0.1(\cos(4\pi r) - 1) & \text{if } 0 < r < 0.5, \\ 1 & \text{if } r \geqslant 0.5, \end{cases}$$

where $r = \sqrt{x^2 + y^2}$. The problem is solved on a $[-1,1] \times [-1,1]$ plane domain.

This case is one-dimensional in nature. Therefore, a 1-D solver is used to compute the "exact solution". The grid number is 5000 which is fine enough to obtain a grid independent solution for this test case. Then the numerical results on a sequence of grids are compared to the "exact" solution. In this calculation, the piecewise bilinear recovery algorithm of [9] is used in the reconstruction procedure. For comparison purpose, this test case is also computed using a Lax–Wendroff type finite volume (LWFV) scheme in which the evolution operator $E_{\Delta t/2}$ in Eq. (6) is constructed by computing the interfacial dependent variables using

$$\mathbf{V}^{n+1/2}_{i+1/2,j} = \frac{1}{2}(\mathbf{V}^n_{i,j} + \mathbf{V}^n_{i+1,j}) - \frac{\Delta t}{2}\left[(\mathbf{A}_1(\tilde{\mathbf{V}})\mathbf{V}_x + \mathbf{A}_2(\tilde{\mathbf{V}})\mathbf{V}_y)^n_{i,j} + (\mathbf{A}_1(\tilde{\mathbf{V}})\mathbf{V}_x + \mathbf{A}_2(\tilde{\mathbf{V}})\mathbf{V}_y)^n_{i+1,j}\right].$$

Tables 1 and 2 depict respectively the computed errors in the L_1 norm for the present scheme and the LWFV scheme at $t = 0.5$. It shows that the present scheme is fully second order and its rate of convergence is higher than the LWFV scheme. Moreover, the L_1 error of the present scheme is 2–3 times smaller than that of the LWFV scheme. Fig. 5 shows the scatter plots of the numerical solutions with respect to r computed by the present FVLEG scheme and the LWFV scheme. The result of the FVLEG scheme is not only closer to the exact solution but also less scattering when comparing with the LWFV scheme. This result indicates that the present scheme is superior than the LWFV scheme in preserving the radial symmetry of the solutions.

The second test case is a double periodic shear layer problem on a $[-1,1] \times [-1,1]$ plane domain with its initial condition given by:

$$\rho = 1.4, p = 4, v = \sin(\pi(x + 1.5)),$$
$$u = \begin{cases} \tanh(15(0.5 + y)) & \text{if } y < 0, \\ \tanh(15(0.5 - y)) & \text{otherwise.} \end{cases}$$

The periodic boundary conditions are applied at all boundaries. Initially, there are two shear layers in the flow field which will produce two vortices as time evolves. In the initial stage of the flow field evolution, the solutions are smooth. After a

Table 1
L_1 errors between the numerical solutions of the FVLEG scheme and the "exact solution" for the two-dimensional radially symmetric flow problem at $t = 0.5$.

Grid number	L_1 error of ρ	Order	L_1 error of ρu	Order	L_1 error of E	Order
40×40	1.40E−03		1.02E−03		1.94E−03	
80×80	3.06E−04	2.20	2.27E−04	2.17	4.28E−04	2.18
160×160	7.09E−05	2.11	5.10E−05	2.15	9.91E−05	2.11
320×320	1.70E−05	2.06	1.20E−05	2.09	2.38E−05	2.06

Table 2
L_1 errors between the numerical solutions of the LWFV scheme and the "exact solution" for the two-dimensional radially symmetric flow problem at $t = 0.5$.

Grid number	L_1 error of ρ	Order	L_1 error of ρu	Order	L_1 error of E	Order
40×40	2.80E−03		2.13E−03		3.95E−03	
80×80	7.77E−04	1.85	6.01E−04	1.83	1.09E−03	1.86
160×160	2.21E−04	1.81	1.59E−04	1.91	3.08E−04	1.82
320×320	5.87E−05	1.91	4.19E−05	1.93	8.17E−05	1.91

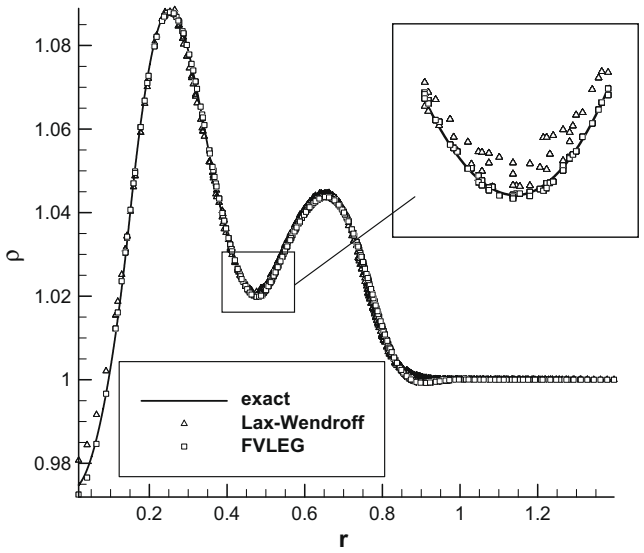

Fig. 5. The scatter plots of the numerical solutions with respect to r for the radially symmetric flow problem.

Table 3
L_1 errors between the numerical solutions of the FVLEG scheme and the "exact solution" for the double periodic shear layer problem at $t = 0.2$.

Grid number	L_1 error of ρ	Order	L_1 error of u	Order	L_1 error of v	Order	L_1 error of p	Order
40×40	4.09E−03		1.22E−02		5.58E−03		1.55E−02	
80×80	9.91E−04	2.04	2.18E−03	2.48	1.42E−03	1.98	3.62E−03	2.10
160×160	2.10E−04	2.24	5.29E−04	2.05	3.62E−04	1.97	7.58E−04	2.25
320×320	4.64E−05	2.18	1.31E−04	2.01	8.58E−05	2.08	1.70E−04	2.16

Table 4
L_1 errors between the numerical solutions of the LWFV scheme and the "exact solution" for the double periodic shear layer problem at $t = 0.2$.

Grid number	L_1 error of ρ	Order	L_1 error of u	Order	L_1 error of v	Order	L_1 error of p	Order
40×40	9.13E−03		3.33E−02		1.70E−02		3.58E−02	
80×80	2.54E−03	1.85	9.53E−03	1.81	5.16E−03	1.72	9.43E−03	1.92
160×160	6.08E−04	2.06	2.49E−03	1.94	1.30E−03	1.99	2.22E−03	2.09
320×320	1.50E−04	2.02	6.24E−04	1.99	3.22E−04	2.01	5.44E−04	2.03

certain time, shock waves will present in the solutions. The numerical results at $t = 0.2$ are used to evaluate the convergence rates of the numerical solutions. At this time, the flow field is still smooth. The test case are computed using the present FVLEG scheme and the LWFV scheme on a sequence of grids from 40×40 to 320×320, and the results on a finer 1280×1280 grid are served as the "exact solution" to evaluate the numerical errors of the solutions on coarser grids. Tables 3 and 4 show, respectively, the computed errors in the L_1 norm for the present scheme and the LWFV scheme. Again, the advantage of the present scheme over the LWFV scheme can be clearly seen in terms of both the order of convergence and the absolute errors.

5.2. Shock capturing capability

In this subsection, we will study the shock capturing capability of the present FVLEG scheme. In this case, the reconstruction procedure of Section 2.3 is used to suppress the numerical oscillations near the flow discontinuities. Fig. 6 shows the numerical results of the second test case in Section 5.1 at $t = 0.5$ when the shock waves have already formed. According to the density contours shown in Fig. 6(a), the discontinuities are well captured with high resolution. In Fig. 6(b), the jumps of the velocity vectors across the shock waves can be seen clearly.

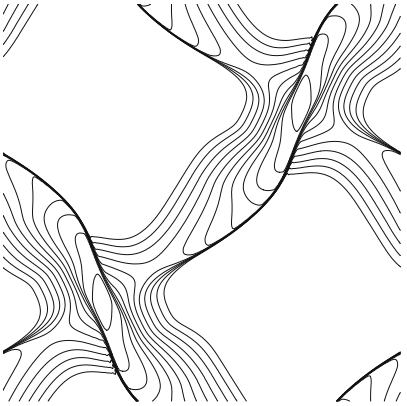

The FVLEG scheme is also applied to solve the two-dimensional Riemann problems which have been established as the benchmark test cases for multi-dimensional solvers. Here we consider two test cases with different initial conditions. For the first one, the initial conditions are [11],

$$\rho = 1.1, \quad u = 0.0, \quad v = 0.0 \quad p = 1.1 \quad \text{if } x > 0, y > 0;$$
$$\rho = 0.5065, \quad u = 0.0, \quad v = 0.8939 \quad p = 0.35 \quad \text{if } x > 0, y < 0;$$
$$\rho = 0.5065, \quad u = 0.8939, \quad v = 0.0 \quad p = 0.35 \quad \text{if } x < 0, y > 0;$$
$$\rho = 1.1, \quad u = 0.8939, \quad v = 0.8939 \quad p = 1.1 \quad \text{if } x < 0, y < 0.$$

For this configuration two forward-moving shocks and two standing slip lines are produced. The numerical solutions in terms of the density contours are shown in Fig. 7 for both the first-order and the second- order FVLEG scheme on a 400×400 grid. The flow structures are correctly captured by the present scheme and the resolution of the present scheme is very satisfactory. It is worthwhile to point out that the present scheme produces very clean slip lines, whereas in [11], some wiggles are present at the slip lines for a second-order FVEG scheme.

For the second two-dimensional Riemann problem, we consider the following initial data:

$$\rho = 0.5313, \quad u = 0.0, \quad v = 0.0 \quad p = 0.4 \quad \text{if } x > 0, y > 0;$$
$$\rho = 1.0, \quad u = 0.0, \quad v = 0.7276 \quad p = 1.0 \quad \text{if } x > 0, y < 0;$$
$$\rho = 1.0, \quad u = 0.7276, \quad v = 0.0 \quad p = 1.0 \quad \text{if } x < 0, y > 0;$$
$$\rho = 0.8, \quad u = 0.0, \quad v = 0.0 \quad p = 1.0 \quad \text{if } x < 0, y < 0.$$

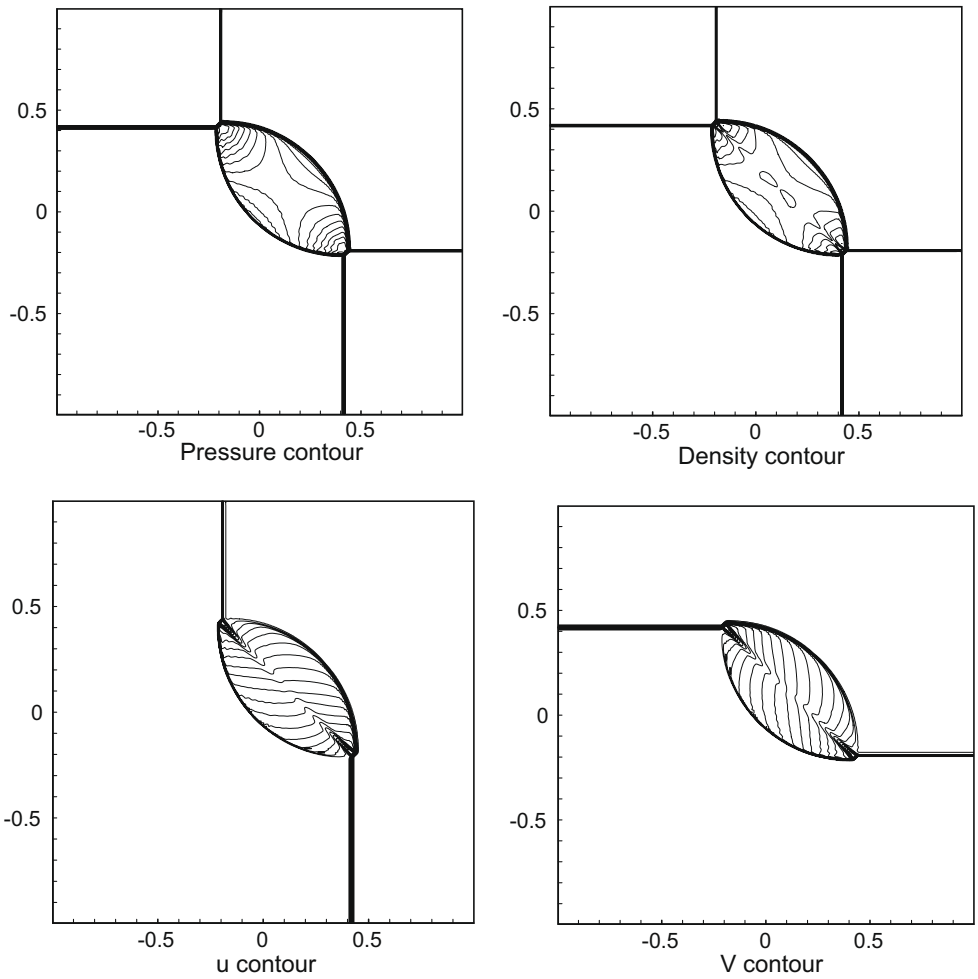

Fig. 8. The contours of the two-dimensional Riemann problem obtained by the FVLEG schemes at $T = 0.25$ on a 400×400 mesh.

The solution consists of two forward-moving shocks and two backward-moving shocks. In Fig. 8, the contours of solution obtained by the second-order FVLEG method are plotted. The Mach reflections in $x = -y$ are well resolved.

6. Conclusions

This paper presents a finite volume local evolution Galerkin scheme (FVLEG) for solving the gas dynamic Euler equations. The FVLEG scheme simplifies the construction and implementation of the FVEG schemes while maintaining the multi-dimensional nature in numerical flux evaluation. The present numerical flux evaluation algorithm is able to be applied on general shaped control volumes for both structured and unstructured grids. The present scheme is a semi-discrete finite volume scheme in which the evaluation of the numerical fluxes is decoupled with the reconstruction procedure. This property makes it straightforward to achieve higher temporal and spatial accuracy. The performance of the proposed scheme is studied by solving several test cases. It is shown that FVLEG scheme can obtain satisfactory numerical result in terms of both accuracy and resolution to flow discontinuities.

Acknowledgment

This work was supported by Project-10572075 of NSFC.

Appendix

This appendix presents the detailed procedure to evaluate θ_{ib} and θ_{ie}. Referring to Fig. A1, we have $P_0 = (x, y, t)$ and $P = (x, y, t + \tau)$. P is the apex of the Mach cone where the interfacial values of the dependent variables will be computed. In this appendix, we consider the case that $\mathbf{r} = (x, y)^T$ is the vertex of the control volume $\Omega_{s,t}$. We denote $\mathbf{e}_1$ and $\mathbf{e}_2$ two unit vec-

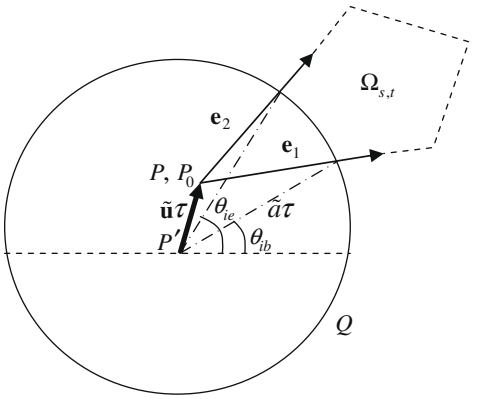

Fig. A1. The schematic sketch for evaluating θ_{ie} and θ_{ib}.

tors corresponding to two rays with their end points at P_0 and aligned, respectively, with two edges of the control volume $\Omega_{s,t}$ with the common vertex P_0. It is further assumed that $\mathbf{e}_1 \times \mathbf{e}_2 > 0$. In practice, there are several control volumes (including $\Omega_{s,t}$) with the common vertex P_0. However, in the appendix, we only consider the contributions of $\Omega_{s,t}$ to the evaluation of Eqs. (42)–(45), and other control volumes can be dealt with exactly the same procedure that will be presented below. We also note that it is not necessary to distinguish the difference in time when dealing with geometrical relations. Therefore, P_0 and P spatially refer to the same point $\mathbf{r} = (x,y)^T$.

The center of the circle $Q(\theta)$ is at $P' = (x - \tilde{u}\tau, y - \tilde{v}\tau, t)$. According to Fig. A1, θ_{ib} or θ_{ie} can be determined by the intersections between $Q(\theta)$ and the ray $\mathbf{e}_1$ or $\mathbf{e}_2$. Denoting the angles of $\mathbf{e}_1$and $\mathbf{e}_2$ with respect the x-axis as α_1, α_2 respectively, we have

$$e_{kx} = \cos\alpha_k, \quad e_{ky} = \sin\alpha_k, \quad k = 1, 2.$$

The parametric equation of the ray corresponding to $\mathbf{e}_k$ ($k = 1,2$) can be written as

$$X = x + l\cos\alpha_k,$$
$$Y = y + l\sin\alpha_k.$$

The equation of $Q(\theta)$ is

$$[X - (x - \tilde{u}\tau)]^2 + [Y - (y - \tilde{v}\tau)]^2 = (\tilde{a}\tau)^2.$$

Therefore, the intersection of ray $\mathbf{e}_k$ with circle Q can be obtained by the solutions of the equation

$$(\tilde{u}\tau + l\cos\alpha_k)^2 + (\tilde{v}\tau + l\sin\alpha_k)^2 = (\tilde{a}\tau)^2,$$

which gives the solutions in terms of the parameter l,

$$l_{k,1} = -\tau(\tilde{u}\cos\alpha_k + \tilde{v}\sin\alpha_k) - \tau\sqrt{\tilde{a}^2 - (\tilde{u}\sin\alpha_k - \tilde{v}\cos\alpha_k)^2},$$
$$l_{k,2} = -\tau(\tilde{u}\cos\alpha_k + \tilde{v}\sin\alpha_k) + \tau\sqrt{\tilde{a}^2 - (\tilde{u}\sin\alpha_k - \tilde{v}\cos\alpha_k)^2}.$$

If $b_k = |\tilde{u}\sin\alpha_k - \tilde{v}\cos\alpha_k| \leqslant \tilde{a}$, the solutions are real. We note that when the solutions $l_{k,l} \geqslant 0$ ($k = 1,2$; $l = 1,2$), there are intersections between the circle Q and ray $\mathbf{e}_k$ at

$$X_{k,l} = x + l_{k,l}\cos\alpha_k,$$
$$Y_{k,l} = y + l_{k,l}\sin\alpha_k.$$

The angle between vector $(X_{k,l} - (x - \tilde{u}\tau), Y_{k,l} - (y - \tilde{v}\tau))^T$ and the x-axis satisfies

$$\cos\theta_{k,l} = \frac{\tilde{u} + l_{k,l}\cos\alpha_k}{\tilde{a}},$$
$$\sin\theta_{k,l} = \frac{\tilde{v} + l_{k,l}\sin\alpha_k}{\tilde{a}}.$$

$\theta_{k,l}$ can thus be determined by

$$\theta_{k,l} = \pi + sign(\sin\theta_{k,l})\left[\arccos\left(\frac{u + l_{k,l}\cos\alpha_i}{a}\right) - \pi\right],$$

where

$$sign(c) = \begin{cases} 1, & c \geqslant 0, \\ -1, & \text{otherwise}. \end{cases}$$

It is apparent that $\theta_{k,l}$ is independent with τ.

We can therefore distinguish the following case.

(1) If $b_k > \tilde{a}$ or $l_{k,1} \leqslant l_{k,2} < 0$, there is no intersection between ray $\mathbf{e}_k$ and circle Q. The number of intersection is $n_k = 0$.
(2) Otherwise if $l_{k,2} \geqslant 0, l_{k,1} < 0$, there is one intersection between ray $\mathbf{e}_k$ and circle Q. The number of intersection is $n_k = 1$.
(3) Otherwise, there are two intersections between ray $\mathbf{e}_k$ and circle Q. The number of intersection is $n_k = 2$.

In order to proceed with the derivation of θ_{ie} and θ_{ib} in Eqs. (42)–(45), we need to determine the relative position between $\mathbf{e}_1$, $\mathbf{e}_2$ and P'. This can be achieved by the following procedure:

(1) If $\tilde{\mathbf{u}} \times \mathbf{e}_1 \geqslant 0$ and $\mathbf{e}_2 \times \tilde{\mathbf{u}} \geqslant 0, P'$ is on the region bounded by $\mathbf{e}_1$ and $\mathbf{e}_2$, or $P' \in \Omega_{s,t}$ in short.
(2) Otherwise, $P' \notin \Omega_{s,t}$.

Using the relations discussed above, we can reach the following conclusion:

(1) If $n_1 = n_2 = 0$ and $P' \notin \Omega_{s,t}$, $\Omega_{s,t}$ has no contribution in Eqs. (42)–(45).
(2) If $n_1 = n_2 = 0$ and $P' \in \Omega_{s,t}$, then $\theta_{ib} = 0$ and $\theta_{ie} = 2\pi$, which means that Eqs. (42)–(45) are determined exclusively by the reconstructions on $\Omega_{s,t}$.
(3) If $n_1 = n_2 = 1$, then $\theta_{ib} = \theta_{12}, \theta_{ie} = \begin{cases} \theta_{22}, & \text{if } \theta_{22} \geqslant \theta_{12} \\ \theta_{22} + 2\pi, & \text{otherwise} \end{cases}$.
(4) If $n_1 = 2$, $n_2 = 0$, then $\theta_{ib} = \theta_{12}, \theta_{ie} = \begin{cases} \theta_{11}, & \text{if } \theta_{11} \geqslant \theta_{12} \\ \theta_{11} + 2\pi, & \text{otherwise} \end{cases}$.
(5) If $n_1 = 0, n_2 = 2$, then $\theta_{ib} = \theta_{21}, \theta_{ie} = \begin{cases} \theta_{22}, & \text{if } \theta_{22} \geqslant \theta_{21} \\ \theta_{22} + 2\pi, & \text{otherwise} \end{cases}$.
(6) If $n_1 = n_2 = 2$, there are two arcs contributing to Eqs. (42)–(45), the staring and ending angles of these two arcs are respectively $\theta^1_{ib} = \theta_{12}, \theta^1_{ie} = \begin{cases} \theta_{22}, & \text{if } \theta_{22} \geqslant \theta_{12} \\ \theta_{22} + 2\pi, & \text{otherwise} \end{cases}$ and $\theta^2_{ib} = \theta_{21}, \theta^2_{ie} = \begin{cases} \theta_{11}, & \text{if } \theta_{11} \geqslant \theta_{21} \\ \theta_{11} + 2\pi, & \text{otherwise} \end{cases}$.

We note that in all cases presented above, the dependent variables corresponding to $Q(\theta_{ib})$ and $Q(\theta_{ie})$ in Eqs. (42)–(45) are $\mathbf{V}_i = \mathbf{V}_{\Omega_{s,t}}(P_0)$ where $\mathbf{V}_{\Omega_{s,t}}$ is the vector of the reconstructed primitive variables on $\Omega_{s,t}$.

References

[1] K.R. Arun, M. Kraft, M. Lukáčová-Medvid'ová, P. Prasad, Finite volume evolution Galerkin method for hyperbolic conservation laws with spatially varying flux functions, J. Comput. Phys. 228 (2009) 565–590.
[2] H. Deconinck, R. Struijs, P. Roe, Fluctuation splitting schemes for the 2D Euler equations, Report 1991-11/AR, Von Karman Institute, Belgium, 1991.
[3] M. Fey, Multidimensional upwinding, Part II. Decomposition of the Euler equations into advection equations, J. Comput. Phys. 143 (1998) 181–199.
[4] S. Godunov, Finite difference methods for numerical computation of discontinuous solutions of the equations of fluid dynamics, Math. Sb. 47 (1959) 271–290.
[5] A. Harten, P. Lax, A random choice finite difference scheme for hyperbolic conservation laws, SIAM J. Numer. Anal. 18 (1981) 289–315.
[6] R.J. LeVeque, Wave propagation algorithms for multi-dimensional hyperbolic systems, J. Comput. Phys. 131 (1997) 327–353.
[7] M. Lukáčová-Medvid'ová, K.W. Morton, G. Warnecke, Evolution Galerkin methods for hyperbolic systems in two space dimensions, Math. Comput. 69 (2000) 1355–1384.
[8] M. Lukáčová-Medvid'ová, K.W. Morton, G. Warnecke, Finite volume evolution Galerkin methods for Euler equations of gas dynamics, Int. J. Numer. Meth. Fluids 40 (2002) 425–434.
[9] M. Lukáčová-Medvid'ová, KW. Morton, G. Warnecke, Finite volume evolution Galerkin (FVEG) methods for hyperbolic problems, SIAM J. Sci. Comput. 26 (1) (2004) 1–30.
[10] M. Lukáčová-Medvid'ová, S. Noelle, M. Kraft, Well-balanced finite volume evolution Galerkin methods for the shallow water equations, J. Comput. Phys. 221 (2007) 122–147.
[11] M. Lukáčová-Medvid'ová, J. Saibertová, G. Warnecke, Finite volume evolution Galerkin methods for nonlinear hyperbolic systems, J. Comput. Phys. 183 (2002) 533–562.
[12] M. Lukáčová-Medvid'ová, J. Saibertová, Finite volume schemes for multi-dimensional hyperbolic systems based on the use of bicharacteristics, Appl. Math. 51 (2006) 205–228.
[13] M. Lukáčová-Medvid'ová, G. Warnecke, Y. Zahaykah, On the stability of evolution Galerkin schemes applied to a two-dimensional wave equation system, SIAM J. Sci. Comput. 44 (4) (2006) 1556–1583.
[14] S. Noelle, The MOT-ICE: a new high-resolution wave-propagation algorithm for multi-dimensional systems of conservative laws based on Fey's method of transport, J. Comput. Phys. 164 (2000) 283–334.
[15] S. Osher, F. Solomon, Upwind difference schemes for hyperbolic systems of conservation laws, Math. Comput. 38 (1982) 339–374.
[16] J. Quirk, A contribution to the great Riemann solver debate, Int. J. Numer. Meth. Fluid Dyn. 18 (1994) 555–574.
[17] P. Roe, Approximate Riemann solvers, parameter vectors, and difference schemes, J. Comput. Phys. 43 (1981) 357–372.
[18] P. Roe, Discrete models for the numerical analysis of time-dependent multidimensional gas dynamics, J. Comput. Phys. 63 (1986) 458–476.
[19] Y.X. Ren, Y.T. Sun, A multi-dimensional upwind scheme for solving Euler and Navier–Stokes equations, J. Comput. Phys. 219 (2006) 391–403.
[20] Y.X. Ren, M. Liu, H.X. Zhang, A characteristic-wise hybrid compact-WENO scheme for solving hyperbolic conservation laws, J. Comput. Phys. 192 (2003) 365–386.
[21] J. Saibertová, Genuinely multidimensional finite volume schemes for systems of conservation laws, Ph.D. Thesis, Technical University Brno, 2003.
[22] B. Van Leer, Towards the ultimate conservative difference scheme V, J. Comput. Phys. 32 (1979) 101–136.
[23] Y. Zahaykah, Evolution Galerkin schemes and discrete boundary conditions for multidimensional first order systems, Ph.D. Thesis, University of Magdeburg, 2002.